

RESEARCH ARTICLE

Open Access

# TiO<sub>2</sub>-graphene oxide nanocomposite as advanced photocatalytic materials

Václav Štengl<sup>1\*</sup>, Snejana Bakardjieva<sup>1</sup>, Tomáš Matys Grygar<sup>1</sup>, Jana Bludská<sup>1</sup> and Martin Kormunda<sup>2</sup>

## Abstract

**Background:** Graphene oxide composites with photocatalysts may exhibit better properties than pure photocatalysts via improvement of their textural and electronic properties.

**Results:** TiO<sub>2</sub>-Graphene Oxide (TiO<sub>2</sub> - GO) nanocomposite was prepared by thermal hydrolysis of suspension with graphene oxide (GO) nanosheets and titania peroxo-complex. The characterization of graphene oxide nanosheets was provided by using an atomic force microscope and Raman spectroscopy. The prepared nanocomposites samples were characterized by Brunauer–Emmett–Teller surface area and Barrett–Joiner–Halenda porosity, X-ray Diffraction, Infrared Spectroscopy, Raman Spectroscopy and Transmission Electron Microscopy. UV/VIS diffuse reflectance spectroscopy was employed to estimate band-gap energies. From the TiO<sub>2</sub> - GO samples, a 300 μm thin layer on a piece of glass 10×15 cm was created. The photocatalytic activity of the prepared layers was assessed from the kinetics of the photocatalytic degradation of butane in the gas phase.

**Conclusions:** The best photocatalytic activity under UV was observed for sample denoted TiGO\_100 ( $k = 0.03012 \text{ h}^{-1}$ ), while sample labeled TiGO\_075 ( $k = 0.00774 \text{ h}^{-1}$ ) demonstrated the best activity under visible light.

**Keywords:** Graphene, Titanium(IV) oxide, Graphene oxide, Photocatalysis

## Introduction

Traditionally, TiO<sub>2</sub> is currently known as the most available and commercially cheapest photocatalyst. It has been well documented that GO is heavily oxygenated graphene that is readily exfoliated in water to yield stable dispersions consisting mostly of single-layer sheets. The use of graphene oxide as the nanoscale substrates for the formation of nanocomposites with metal oxides is widely explored due to an idea to obtain a hybrid which could be combined both properties of GO as fascinating paper-shape material and the features of single nano-sized metal oxide particles.

Recent studies concentrate on the preparation and applications of GO modified photocatalyst because their large specific surface area and high activity in most catalytic processes. Krishnamoorthy et al. [1] presented an article where photocatalytic characteristics and properties of graphene oxide were investigated by measuring the reduction rate of resazurin into resorufin as a function of

UV irradiation time. The synthesis and physicochemical characterization of titanium oxide nanoparticle-graphene oxide (TiO<sub>2</sub>-GO) and titanium oxide nanoparticle-reduced graphene oxide (TiO<sub>2</sub>-RGO) composites were early provided and emphasized on the different synthetic strategies for the preparation of graphene-TiO<sub>2</sub> materials. For example, TiO<sub>2</sub>-GO materials have been prepared via the hydrolysis of TiF<sub>4</sub> at 60°C for 24 h in the presence of an aqueous dispersion of graphene oxide (GO). The reaction proceeded to yield an insoluble material that is composed of TiO<sub>2</sub> and GO [2].

In another strategy graphene oxide/TiO<sub>2</sub> composites were prepared by using TiCl<sub>3</sub> and graphene oxide as reactants. The concentration of graphene oxide in starting solution played an important role in photoelectronic and photocatalytic performance of graphene oxide/TiO<sub>2</sub> composites. In this way either a p-type or n-type semiconductive graphene oxide/TiO<sub>2</sub> composites were synthesized. These semiconductors were excited by visible light with wavelengths longer than 510 nm and acted as sensitizers in graphene TiO<sub>2</sub> composites [3].

TiO<sub>2</sub>-Graphene Oxide intercalated composite has been successfully prepared at low temperature (80°C) with

\* Correspondence: stengl@iic.cas.cz

<sup>1</sup>Department of Solid State Chemistry, Institute of Inorganic Chemistry AS CR v.v.i., Rež 250 68, Czech Republic

Full list of author information is available at the end of the article

graphite oxide and titanium sulfate  $\text{Ti}(\text{SO}_4)_2$  as initial reactants. Graphite oxide was firstly exfoliated by NaOH and formed single and multi-layered graphite oxide mixture which can be defined as graphene oxide,  $[\text{TiO}]^{2+}$  induced by the hydrolysis of  $\text{Ti}(\text{SO}_4)_2$  diffused into graphene oxide interlayer by electrostatic attraction [4].

Recently, Min et al. [5] presented a novel dye-sensitized photocatalytic system for photochemical energy conversion employing reduced graphene oxide (RGO) as a catalyst scaffold and an efficient electron relay mediator between photosensitizer and catalyst. Under visible light irradiation ( $\lambda = 420$  nm), the photocatalyst of Eosin Y sensitized RGO with dispersed Pt nanoparticles exhibited highly efficient activity for hydrogen evolution from water reduction.

A new technique for producing of novel solvent-exfoliated graphene- $\text{TiO}_2$  nanocomposites was published [6], which are then compared to previously reported reduced graphene oxide- $\text{TiO}_2$  nanocomposites in an effort to elucidate the role of graphene and its defects in the photocatalytic reduction of  $\text{CO}_2$  to  $\text{CH}_4$ . Another novel method [7] was developed to synthesize graphite oxide/ $\text{TiO}_2$  composites as a highly efficient photocatalyst by in situ depositing  $\text{TiO}_2$  nanoparticles on graphene oxide nano-sheets by a liquid phase deposition, followed by a calcination treatment at  $200^\circ\text{C}$ .

In our previous work [8], we reported on nonstoichiometric  $\text{TiO}_2$ -graphene oxide nanocomposite, which was prepared by thermal hydrolysis of suspension with graphene oxide nanosheets and titania peroxo-complex. It should be mentioned that we are able to produce pure graphene nanosheets in large quantity from natural graphite by using high intensity cavitation field in the high-pressure ultrasonic reactor. Graphene oxide sheets, prepared by such safe and friendly method, can be used as a good support for  $\text{TiO}_2$  to enhance its photocatalytic activity. In this paper, we reported on an "one-pot" thermal hydrolysis of titanium peroxo-complexes in the presence of graphene oxide in aqueous solution. Our "hydrogen peroxide route" is based on hydrolysis of  $\text{Ti}(\text{IV})$  sulfate, next treatment of the resulting gel by hydrogen peroxide, and thermal decomposition of so formed peroxo-titanate under reflux at ambient pressure producing directly the  $\text{TiO}_2$ -GO photocatalyst. The relative photocatalytic activity of the as-prepared thin layers of titania/graphene nanocomposite in poly(hydroxyethyl methacrylate) was assessed by the photocatalytic decomposition of butane under UV and visible light.

#### Preparation $\text{TiO}_2$ - GO nanocomposite

All chemical reagents used in the present experiments were obtained from commercial sources and used without further purification. Titanium oxo-sulfate  $\text{TiOSO}_4$ , hydrogen peroxide  $\text{H}_2\text{O}_2$ , ethylene glycol  $\text{OHCH}_2\text{CH}_2\text{OH}$  and

ammonium hydroxide  $\text{NH}_4\text{OH}$  were supplied by Sigma-Aldrich. Graphene was produced in large quantity from natural graphite (Koh-i-noor Grafite Ltd. Czech republic) using high intensity cavitation field in a pressure batch-ultrasonic reactor (UIP 2000hd, 20 kHz, 2000 W, Hielscher Ultrasonics GmbH) [9].

Graphene oxide was prepared by our safety method, a 60 ml of  $\text{H}_2\text{SO}_4$  and 10 ml of  $\text{H}_3\text{PO}_4$ , 1 g of graphene and 3 g of  $\text{KMnO}_4$  were mixed in round bottom flask. The reaction was then heated to  $40^\circ\text{C}$  and stirred for 6 hours and pink squash suspension was obtained. Subsequently was poured onto ice with 200 ml of 30%  $\text{H}_2\text{O}_2$ . The pink squash suspension quickly changed to lemon-like yellow suspension. The whole reaction product was purged by dialysis (Spectra/Por 3 dialysis membrane), washed with ethanol and dried at  $105^\circ\text{C}$ .

In the typical procedure of  $\text{TiO}_2$  - GO nanocomposite preparation, 100 ml of 1.6 M titanium oxo-sulfate ( $\text{TiOSO}_4$ ) was hydrolyzed by slow addition of ammonium hydroxide solution (10%) under constant stirring at temperature of  $0^\circ\text{C}$  in ice bath. The stirring last until the reaction mixture reaches pH 8.0. The obtained white precipitate was separated by filtration. The consequent depuration of sulfate ions from precipitate with distilled water was confirmed by the  $\text{BaCl}_2$ . The wet precipitate is mixed with 100 ml of 15% hydrogen peroxide solution; thereby a yellow solution of titania peroxo-complex is obtained.

Well defined quantity (see Table 1) of GO nanosheets was dispersed using ultrasound in water, added to the yellow precursor of titania peroxo-complex and annealed at a heated mantle in a round-bottom flask with a reflux cooler at  $100^\circ\text{C}$  for 48 hours. The originated blue  $\text{TiO}_2$  - GO nanocomposite was filtered off and dried at  $105^\circ\text{C}$ . Ten samples of  $\text{TiO}_2$ -GO nanocomposites doped as  $\text{TiGO\_XXX}$ , where XXX are grams of GO, were prepared.

The prepared  $\text{TiO}_2$  - GO nanocomposite powder (2 g) was dispersed in a mixture of 5 ml poly(hydroxyethyl methacrylate) and 10 ml of ethanol. From this suspension, a  $300\ \mu\text{m}$  thin layer on a piece of glass,  $100 \times 150$  mm was created.

#### Characterisation methods

Diffraction patterns were collected with diffractometer PANalytical X'Pert PRO equipped with conventional X-ray tube (Cu  $K\alpha$  radiation, 40 kV, 30 mA) and a linear position sensitive detector PIXcel with an anti-scatter shield. A programmable divergence slit set to a fixed value of 0.5 deg, Soller slits of 0.02 rad and mask of 15 mm were used in the primary beam. A programmable anti-scatter slit set to fixed value of 0.5 deg, Soller slit of 0.02 rad and Ni beta-filter were used in the diffracted beam. Qualitative analysis was performed with the DiffracPlus Eva software package (Bruker AXS, Germany) using the JCPDS PDF-2

**Table 1 Sample composition, crystallite size, BET a total pore volume of prepared samples**

Sample	Graphene oxide [g]	Crystallite size [nm]	Cell parameter a [Å]	Cell parameter c [Å]	BET [m <sup>2</sup> g <sup>-1</sup> ]	Total pore volume [cm <sup>3</sup> g <sup>-1</sup> ]
TiGO_001	0.005	49.6	3.7963(2)	9.5144(5)	100.2	0.6530
TiGO_005	0.001	51.9	3.7968(4)	9.5121(4)	151.4	0.7846
TiGO_010	0.01	52.2	3.7970(2)	9.5121(6)	195.7	1.4668
TiGO_050	0.05	34.5	3.7970(3)	9.5086(8)	185.7	0.623
TiGO_075	0.075	34.5	3.7973(2)	9.5077(7)	119.2	0.6501
TiGO_100	0.100	32.1	3.7973(6)	9.5060(4)	168.4	0.6687
TiGO_200	0.200	35.0	3.7971(4)	9.5047(5)	178.0	0.6247
TiGO_300	0.300	46.7	3.7954(5)	9.5118(7)	78.9	0.618
TiGO_400	0.400	43.6	3.7954(2)	9.5106(6)	68.6	0.5545
TiGO_500	0.500	39.1	3.7955(6)	9.5095(8)	78.1	0.6089

database [10]. For quantitative analysis of XRD patterns we used Diffrac-Plus Topas (Bruker AXS, Germany, version 4.1) with structural models based on ICSD database [11]. This program permits to estimate the weight fractions of crystalline phases and mean coherence length by means of Rietveld refinement procedure.

AFM images were obtained using an NTEGRA Aura (NT-MTD) microscope. A sample of the diluted dispersion was placed on synthetic mica as an atomically smooth support and evaporated at room temperature. The measurements were performed in air at room temperature in non contact mode, with Si tips of the 1650–00 type at resonance frequencies ranging from 180 to 240 kHz.

The morphology of sample powders was inspected by transmission electron microscopy (TEM) and the crystal structure was analyzed by electron diffraction (ED) using a 200 kV TEM microscope JEOL 2010 F. As specimen support for TEM investigations a microscopic copper grid covered by a thin transparent carbon film was used. The samples were studied in both bright field and by electron diffraction with a selecting aperture (SAED) mode at an acceleration voltage of 200 kV.

The surface areas of samples were determined from nitrogen adsorption–desorption isotherms at liquid nitrogen temperature using a Coulter SA3100 instrument with out-gas 15 min at 150°C. The Brunauer–Emmett–Teller (BET) method was used for surface area calculation [12], the pore size distribution (pore diameter, pore volume and micropore surface area of the samples) was determined by the Barrett–Joyner–Halenda (BJH) method [13].

The Raman spectra were acquired with DXR Raman microscope (Thermo Scientific) with 532 nm (6 mW) laser, 32 two-second scans were accumulated with laser 532 nm (6 mW) under 10× objective of Olympus microscope.

Infrared spectra were recorded by using Thermo-Nicolet Nexus 670 FT-IR spectrometer approximately in 4000–500 and 500–50 cm<sup>-1</sup>, respectively, with single-

reflection horizontal accessory on Si crystal. The samples were mixed with KBr and pressed to conventional pellets at ambient conditions and measured in the transmission mode.

XPS apparatus was equipped with SPECS X-Ray XR50 (Al cathode 1486.6 eV) and SPECS PHOIBOS 100 Hemispheric Analyzer with 5-channels detector. A background pressure in XPS during the measurements was under 2×10<sup>-8</sup> mbar. XPS survey-scan spectra were made at pass energy of 40 eV; the energy resolution was set to 0.5 eV. While individual high-resolution spectra were taken at pass energy of 10 eV with 0.05 eV energy steps. A software tool CasaXPS was used to fit high-resolution multi components peaks. The proper surface charge compensation was done by fitting C-C, C-H component of C 1 s peak to reference binding energy 284.5 eV. The atomic concentration of compounds was evaluated with relative sensitivity factors (RSF) defined in standard table of CasaXPS software.

Diffuse reflectance UV/VIS spectra for evaluation of photo-physical properties were recorded in the diffuse reflectance mode (R) and transformed to absorption spectra through the Kubelka-Munk function [14]. A Perkin Elmer Lambda 35 spectrometer equipped with a Labsphere RSAPE- 20 integration sphere with BaSO<sub>4</sub> as a standard was used. The reflectance data were obtained as relative percentage reflectance to a non absorbing material (BaSO<sub>4</sub>) which can optically diffuse light.

Kinetics of the photocatalytic degradation of butane (0.87%) was measured by using a home-made stainless steel batch photo-reactor [15] with a Narva black-light fluorescent lamp at wavelength 365 nm and warm-white fluorescent lamp at wavelength up to 400 nm (input power 8 W, light intensity 6.3 mW cm<sup>-2</sup>). The gas concentration was measured with the use of Quadrupole Mass Spectrometer JEOL JMS-Q100GC and gas chromatograph Agilent 6890 N. A high-resolution gas chromatography column (19091P-QO4, J&W Scientific) was used. Samples were taken from the reactor automatically through the

sampling valve (6-port external volume sample injector VICI, Valco Instruments Co. Inc.) in a time interval of 2 hours.

Blank tests (a layer of poly(hydroxyethyl methacrylate) without titania) were performed in order to establish the effect of photolysis and catalysis on the conversion of butane. The UV irradiation detects that there was none or immeasurable conversion of butane, as a testing gas, into CO and/or CO<sub>2</sub>, and consequently neither butane absorbed on the poly(hydroxyethyl methacrylate) matrix. The injection volume of butane into the photoreactor was 30 ml.

## Results and discussion

Early published experimental XRD pattern of graphene oxide demonstrated arising of strong 001 reflection peak at  $2\theta \sim 10^\circ$  with a basal spacing of  $d_{001} = 6.33 \text{ \AA}$  [16]. We calculated d-spacing of sample prepared during our experiment (see Figure 1a) such as GO  $d_{001} = 6.718 \text{ \AA}$  which is in good agreement with published results [16,17].

The Figure 1b shows X-ray diffraction patterns of TiO<sub>2</sub>-GO nanocomposites. All samples show only the anatase phase (PDF 21-1272). Higher concentrations of GO (samples TiGO\_300 and TiGO\_400) probably lead to

partial reduction of GO to graphene and a weak peak at  $2\theta = 26.50^\circ$  appears (see arrow G). Nevertheless, the intensity of graphene X-ray lines is under possibility for quality Rietveld refinement. Furthermore, in the position at  $2\theta \sim 10\text{-}12^\circ$  (see arrow GO), there is an obvious hint of GO peak, which is due to the small particle size and its concentration featureless.

Crystallite size, a and c cell parameters of anatase, calculated by the Rietveld refinement procedure using Topas v.4.2 programme, based on the full width at half-maximum of the peak at  $25.4^\circ$  are presented in Table 1; the crystallite size is in range from  $\sim 32$  to  $52 \text{ nm}$ . The cell parameters of pure anatase are  $a = 3.7845 \text{ \AA}$  and  $c = 9.5143 \text{ \AA}$ ; an increasing of lattice parameters a and c for the titania/graphene oxide nanocomposite is expected to occur if some of the Ti<sup>4+</sup> are transformed to Ti<sup>3+</sup>, because of the larger ionic radius of Ti<sup>3+</sup> ( $0.670 \text{ \AA}$ ) compared to Ti<sup>4+</sup> ( $0.605 \text{ \AA}$ ) [18].

Atomic force microscopy and electron transmission microscopy were used to determine quality of delamination of graphene oxide (GO) used for preparation TiO<sub>2</sub>-GO nanocomposite.

In our previously work we have been demonstrated that the thermal hydrolysis of titania peroxy-complex leads

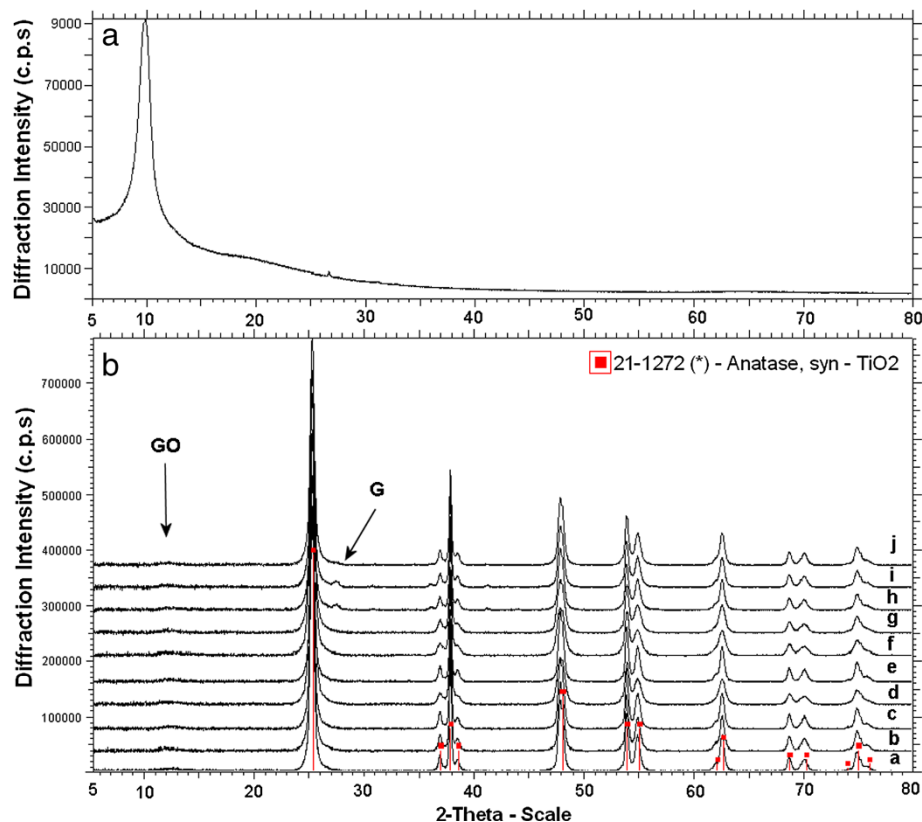


**Figure 1** a The XRD pattern of graphene oxide. b The XRD patterns of TiO<sub>2</sub>-GO nanocomposites, diffraction line a) TiGO\_001, b) TiGO\_005, c) TiGO\_010, d) TiGO\_050, e) TiGO\_075, f) TiGO\_100, g) TiGO\_200, h) TiGO\_300, i) TiGO\_400 and j) TiGO\_500.

to spindle-like particles [19]. Our experiments were confirmed that direct interaction between  $\text{TiO}_2$  nanoparticles and graphene oxide sheet prevents the re-aggregation of the sheets of graphene oxide. The TEM images of GO prepared by modified oxidation method is presented in Figure 2a. It follows from the picture, that GO formed big smooth plates of size  $\sim 5 \times 5 \mu\text{m}$ . Figure 2b shows TEM images of  $\text{TiO}_2$ -GO nanocomposite and demonstrates that  $\text{TiO}_2$  nanoparticles were dispersed uniformly on the graphene plane.

Figure 3 shows AFM images of GO with a thickness of 0.87 nm according to cross-sectional analysis, which is comparable with the interlayer spacing 0.91 nm of GO measured by X-ray powder diffraction (see Figure 1a). These results indicate that the exfoliation of graphite oxide down to monolayer sheets of GO is successfully obtained [16].

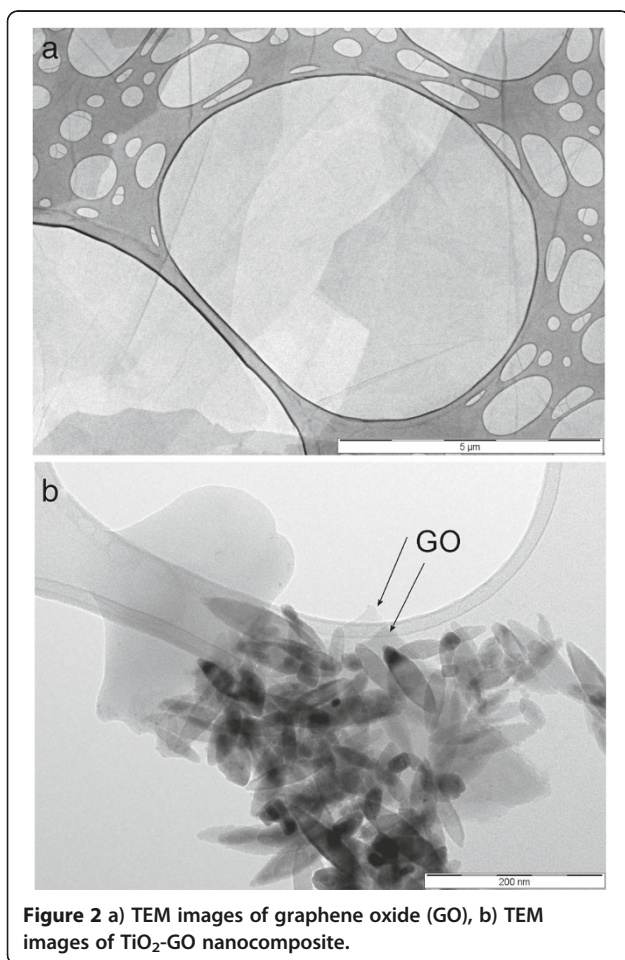
The specific surface area of the prepared  $\text{TiO}_2$ -GO nanocomposites calculated by the multi-point Brunauer-Emmett-Teller (BET) method and total pore volume are listed in Table 1. A typical Barrett-Joyner-Halenda (BJH) pore-size distribution plot and nitrogen adsorption/desorption isotherms are shown in Figure 4. According to

IUPAC notation [20], microporous and macroporous materials have pore diameters smaller than 2 and greater than 50 nm, respectively; the mesoporous category thus lies in the middle. As for all the titania/graphene nanocomposites, the isotherm form corresponds to that of type IV isotherm classification and the type E hysteresis loop is in agreement with the De Boer classification attributed to mesoporous solids [21]. The maximum of average pore size lies between 20 and 35 nm and all prepared  $\text{TiO}_2$ -GO nanocomposites have mesoporous texture. With increasing content of GO in the composite decreasing trend of specific surface area is obvious (see Table 1). This may be due to agglomeration GO, which occurs at higher concentrations. Graphene oxide nanosheets are coated with titania nanoparticles. Therefore when the surface area of  $\text{TiO}_2$ -GO nanocomposites is measured, its size is dominantly determined by surface properties of anatase nanoparticles. For this reason, relatively low specific surface of the  $\text{TiO}_2$ -GO nanocomposites ( $200 \text{ m}^2\text{g}^{-1}$ ) was found compared to the theoretical value of the graphene and graphene oxide, respectively. Nevertheless mesoporous  $\text{TiO}_2$ -graphene oxide nanocomposites have specific surface area in interval  $\sim 80$ – $200 \text{ m}^2\text{g}^{-1}$  being considerably larger than those of P25 and similarly prepared neat  $\text{TiO}_2$  particles without using graphene oxide.

Raman spectroscopy is a powerful tool to characterize the crystalline quality of graphene or GO. Additional file 1: Figure S1 shows the Raman spectrum of GO. In case of thermal hydrolysis of titania peroxy-complexes in the presence of GO there is no reduction of GO. Due to the bluish coloration of samples can be assumed, on the contrary, that there is reduction of  $\text{Ti}^{4+}$  to  $\text{Ti}^{3+}$  [22]. However, if there is a reduction of  $\text{Ti}^{4+}$ , somewhere an oxidation must occur, and it is probably on the graphene skeleton in free positions of  $\Pi$  bonds. Following oxidation of graphene due to reduction of  $\text{Ti}^{4+}$  corresponds to an increase of intensity of Raman bands GO in the nano-composite  $\text{TiO}_2$ -GO.

In our Raman spectrum, the G band is broadened and shifted slightly to  $1605 \text{ cm}^{-1}$ , whereas the intensity of the D band at  $1350 \text{ cm}^{-1}$  increases substantially. Increased background of the spectrum is caused by the sample fluorescence. G band is common to all  $\text{sp}^2$  carbon forms and provides information on the in-plane vibration of  $\text{sp}^2$  bonded carbon atoms and the D band suggests the presence of  $\text{sp}^3$  defects [3].

The Raman spectra of series nanocomposites  $\text{TiO}_2$ -GO is presented in Figure 5. The specific vibration modes are located at  $144 \text{ cm}^{-1}$  (Eg),  $396 \text{ cm}^{-1}$  (B1g),  $512 \text{ cm}^{-1}$  (B1g + A1g) and  $631 \text{ cm}^{-1}$  (Eg) indicating the presence of the anatase phase in all of these samples. The D bands of GO are located at  $1349 \text{ cm}^{-1}$  and G band at  $1601 \text{ cm}^{-1}$ . With increasing concentrations of GO the intensity of both



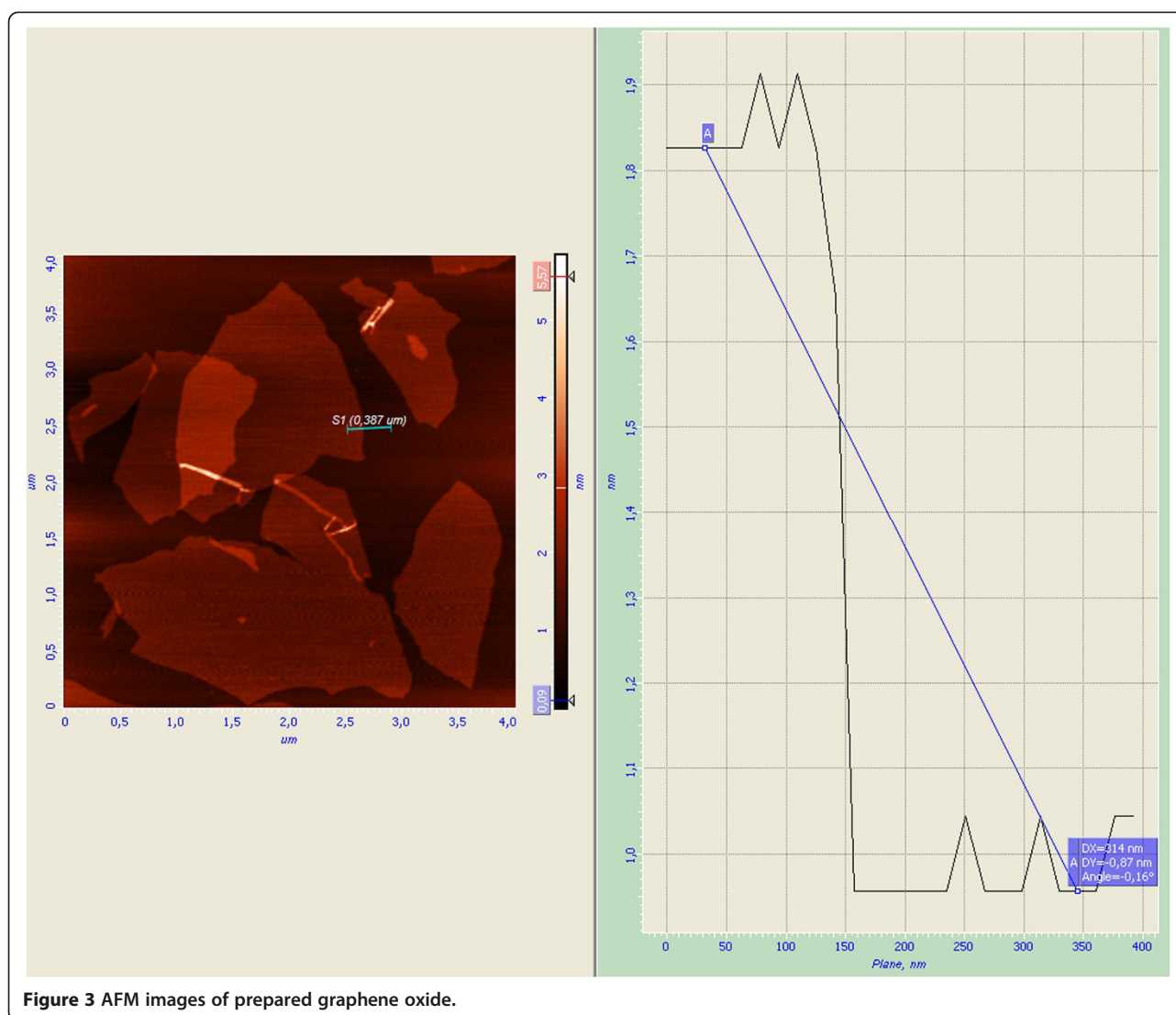


**Figure 3** AFM images of prepared graphene oxide.

bands also increases. The background of the sample labeled TiGO\_075 is increased by the sample fluorescence.

High resolution XPS spectra were accumulated 10 times to enhance the signal and to noise ratio, and are presented in Figure 6. The composition of the TiO<sub>2</sub>-GO nanocomposites was evaluated from the high resolution spectra of O 1 s, C 1 s and Ti 2p. The compositions are summarized in the Additional file 1: Table 1. The O/Ti ratio was evaluated and the results show over stoichiometric values. The high O/Ti ratio can be partially explained by the fact that the O1s spectra show a main peak at 529.7 eV with a shoulder at about ~531.4 eV. The peak at 529.7 eV is assigned to oxygen lattice, while the shoulder may be attributed to oxygen in adsorbed hydroxyl groups.

The binding energy calibration was made on C-C component of C 1 s peak after a deconvolution process. The intensity of C 1 s peak is rather small and the signal is noisy, but the C 1 s peak was fitted by two main

components to represent C-C/C-H bond at binding energies about 284.5 eV and C = O bond at higher binding energies about 288 eV. The C = O bond was expected because it is a part of the graphene oxide precursor. Furthermore, during reaction of Ti(SO<sub>4</sub>)<sub>2</sub> with GO, plenty of oxygen-containing groups, such as C = O located in the interlayer of graphene oxide were consumed during the nucleation and growth of TiO<sub>2</sub> crystallites, which means graphene oxide has been partly reduced [4]. The oxygen-containing groups on the graphene oxide can interact with titanium hydroxide complex and the TiO<sub>2</sub> nanoparticles, resulting in hydrogen bonds between them [23].

The ratio between both bonds was almost identical on both samples (about 73%) and had C-C/C-H character; therefore it can be expected that the carbon comes from the precursor rather than from additional contaminations. The other expected bonds as O = C-OH and C-OH were neglected because of the weak signal [24].

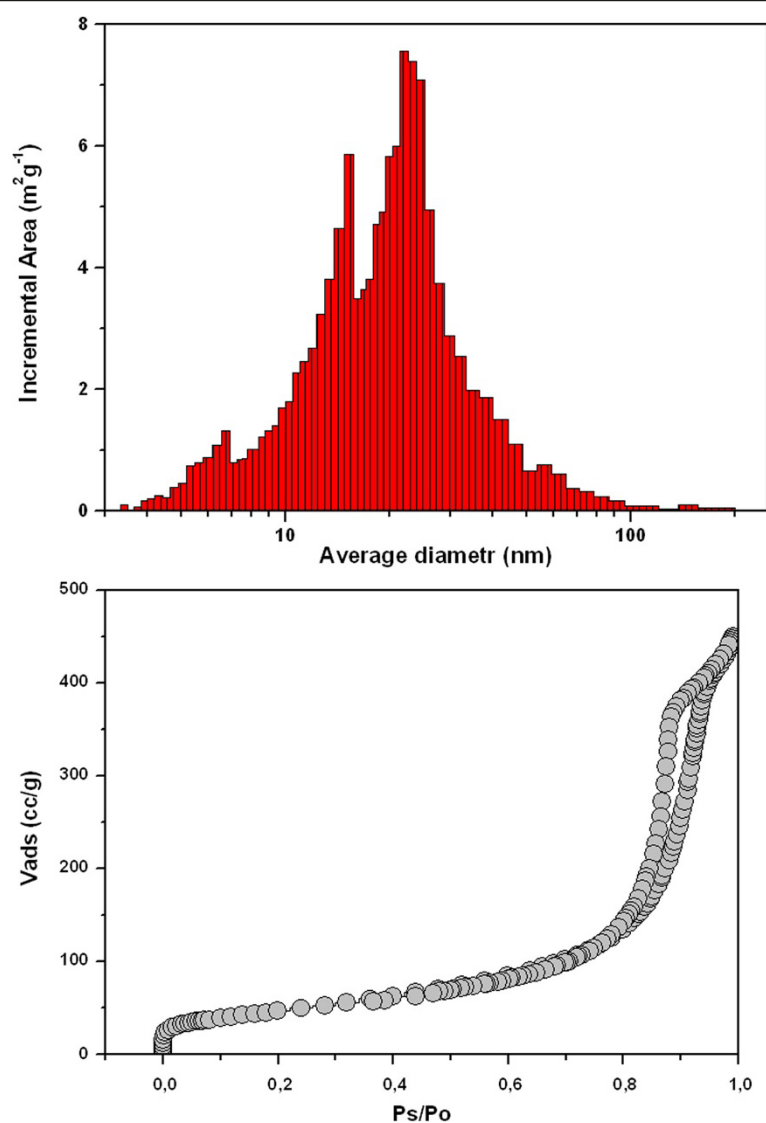


**Figure 4** Dependence of pore area on pore diameter and nitrogen adsorption/desorption isotherms of TiO<sub>2</sub>-GO nanocomposite.

The Ti 2p<sub>3/2</sub> and Ti 2p<sub>1/2</sub> were identified at binding energies of 458.5 and 464.1 eV, respectively. The position of Ti 2p peaks corresponds to the literature reported values and also to the FWHM values about 1.6 eV for Ti 2p<sub>3/2</sub> and 2.4 eV for Ti 2p<sub>1/2</sub>, which are reasonable for single peak character. The Ti is probably bonded in the TiO<sub>2</sub>. The equal area/RFS ratios were found on both spin states within precision about 10%. The limited precision is due to the background removal process when the Shirley background was used. The peak positions and the FWHM were found to be practically identical for all investigated samples.

The Additional file 1: Figure S2 shows the IR spectrum of the TiO<sub>2</sub>-GO nanocomposite prepared by thermal hydrolysis of titania peroxo-complexes. The broad absorption peaks about 3427 cm<sup>-1</sup>, and the band at 1631 cm<sup>-1</sup>

correspond to the surface absorbed water and the hydroxyl groups [25]. The band at 1384 cm<sup>-1</sup> can be assigned to hydroxyl C-OH and that at 1258 cm<sup>-1</sup> to epoxide C-O-C [26]. The band at 650 cm<sup>-1</sup> is most probably related to the Ti-O vibration modes of the Ti<sup>3+</sup>-O-Ti<sup>4+</sup> framework [27].

The Additional file 1: Figure S3 presents the UV-vis absorption spectra of the TiO<sub>2</sub>-GO nanocomposite. The presence of different amounts of GO influences the optical properties of light absorption significantly. With increasing GO content in the nanocomposite light absorption intensity in the UV region grows and a red shift to higher wavelength in the absorption edge at about 400 nm also observed [8]. Increased background in the area 400–800 nm is caused by incorporation of GO into the matrix of TiO<sub>2</sub> [28] and partially also by presence of Ti<sup>3+</sup>.

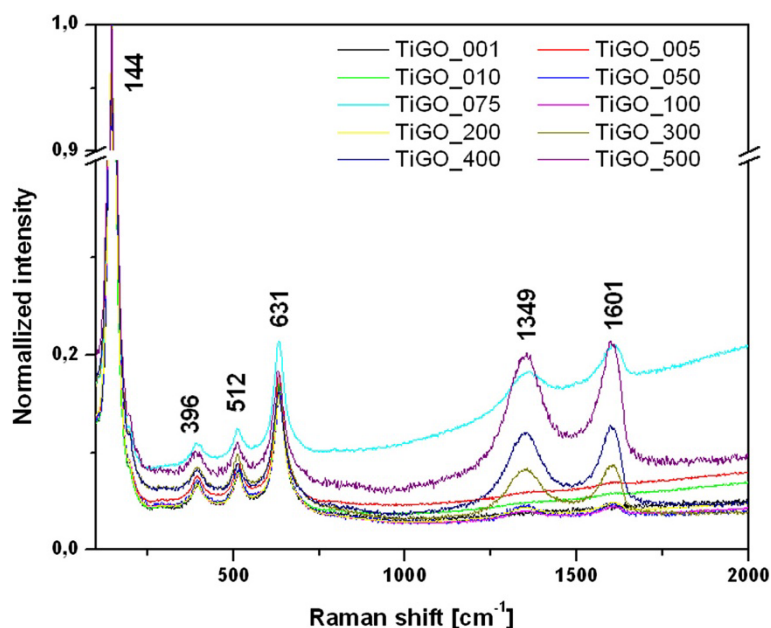


**Figure 5** The Raman spectra of TiO<sub>2</sub>-GO composites.

According to the equation for band gap:

$$\alpha h\nu = B(h\nu - E_{bg})^2 \quad (1)$$

where  $\alpha = (1-R)^2/2R$ ,  $R$  is the reflectance of the "infinitely thick" layer of the solid [29],  $B$  is absorption coefficient and  $h\nu$  is the photon energy in eV. Figure 7 plots the relationship of  $(\alpha h\nu)^{1/2}$  versus photon energy ( $h\nu = 1239/\lambda$ ) [30,31], which shows that the band gap of pure TiO<sub>2</sub> is 3.20 eV, [32] whereas the band gap of the TiO<sub>2</sub>-GO nanocomposite has been reduced from value 3.15 eV (sample TiGO\_001) to value <2.50 eV for sample TiGO\_100. The band-gaps of samples TiGO\_200 to TiGO\_500 are impossible to be identified because the absorption edges for TiO<sub>2</sub> entirely overlapped with those for GO.

The effect of oxidation time variation on the electronic, physical and chemical properties of GO was investigated and it was found that the bandgap of GO increased with oxygen content of the GO material [33]. GO has a bandgap between 1.7 and 4.3 eV in dependence on the preparation method, and it is tunable in the interval 1.9 – 2.6 eV in the range of the visible spectrum as required for efficient photocatalysis.

Graphene oxide is non-stoichiometric material, which retains the lamellar structure of graphite. After treatment in the presence of strong acids and oxidation agents, many oxygen-containing groups such as carboxyl (C–OOH), hydroxyl (C–OH), epoxide (C–O–C) become covalently attached to its layers surfaces. In our experiment GO reacted in the presence of Ti-peroxo-complex, and

some functional group such as (–OH, –COOH) on the GO surface were removed. We can suppose that some unpaired  $\pi$ –electrons bonded with the free electrons on the surface TiO<sub>2</sub> to form a Ti–O–C structure, which then shifted up the valence band edge and reduce d the band gap [34].

On another hand after the photoactivation of titanium dioxide the electrons can easily transfer to the graphene-nanosheets and photoinduced holes migrate into titania; recombination of  $e^-$  and  $h^+$  is strongly reduced, which increases the process yield.

The photocatalytic activity of the as-prepared layered of TiO<sub>2</sub>-GO nanocomposites were assessed from the kinetics of the photocatalytic degradation of butane in the oxygen atmosphere. Photocatalytic oxidation of butane are based on the following overall reactions [35]:



Before each measurement, the photocatalytic reactor is evacuated, then rinsed with the O<sub>2</sub> and the measurement is run. If the measured gas chromatogram shows only the oxygen peak at retention time 1.52 min then a gas for the photocatalytic decomposition (in our case the butane) can be injected. After measuring the subsequent chromatogram, peaks for the oxygen and the butane are marked each by value of 1. The value of gases, which are expected to be formed due to photo-activity of the TiO<sub>2</sub>-GO nanocomposite (CO, CO<sub>2</sub>) are assigned each by value 0. By this normalization of input data is performed and the measurement with time period of 2 hours can be started.

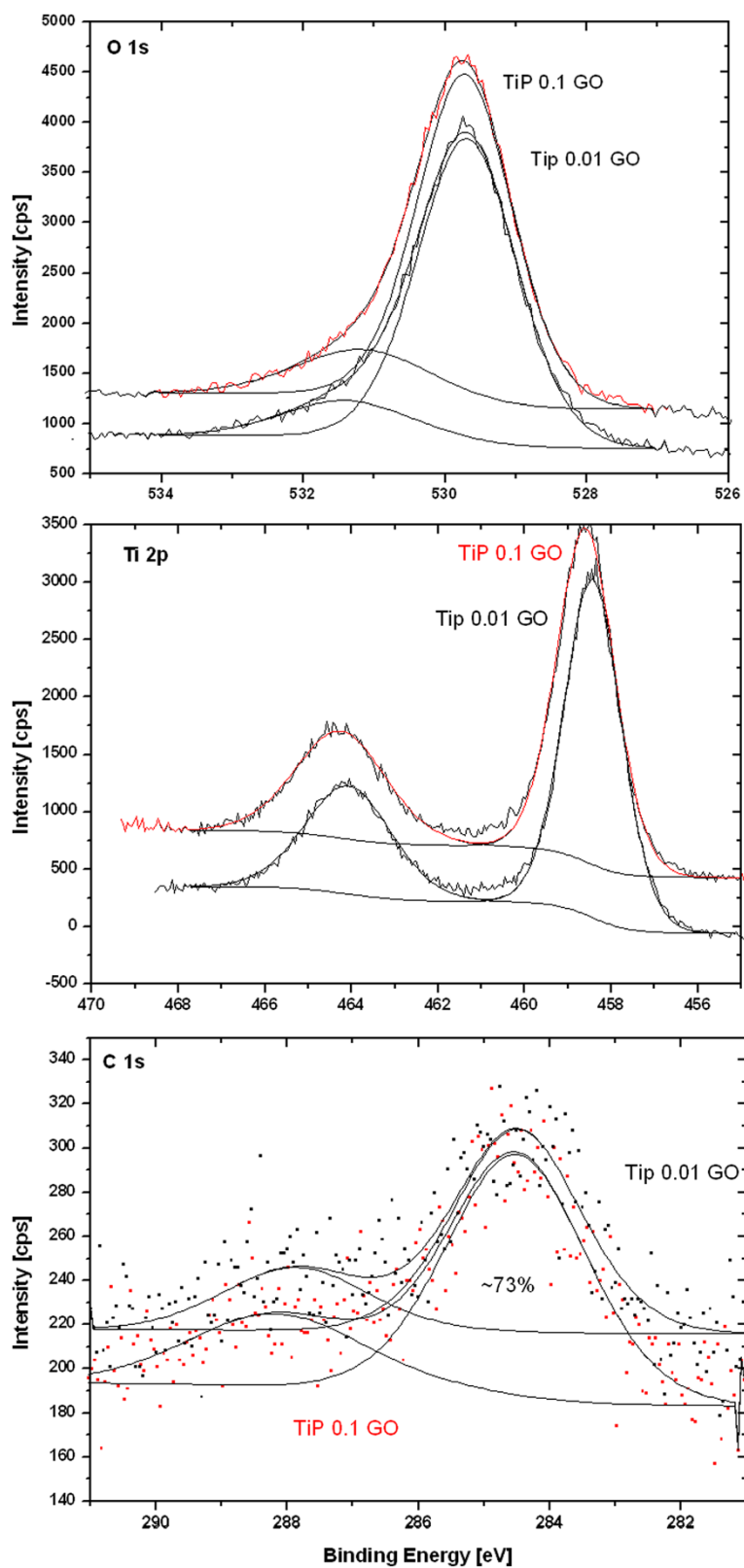


**Figure 6** High resolution XPS spectra of TiO<sub>2</sub>-GO composites.

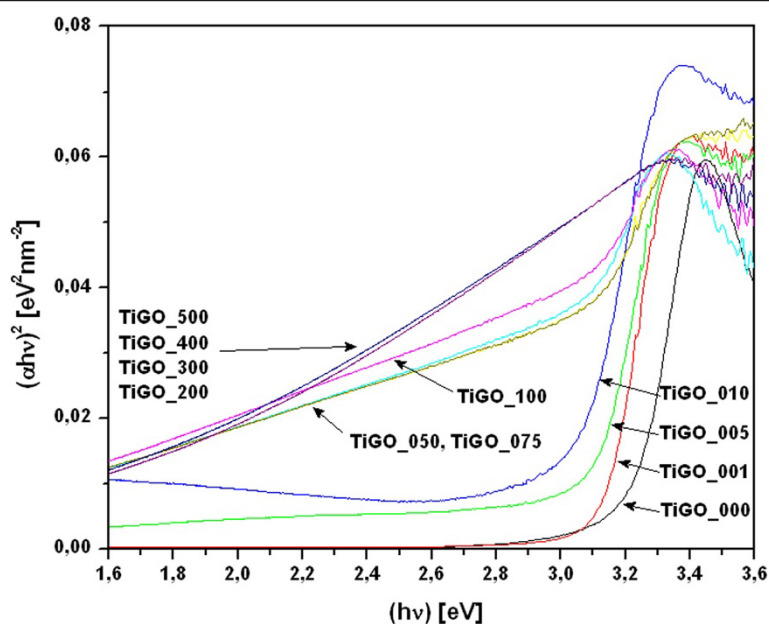


**Figure 7** Band-gap energy ( $h\nu$ ) of  $\text{TiO}_2$ -GO composites.

In a typical chromatograph of the effluent obtained from butane photocatalytic degradation only oxygen, carbon monoxide, carbon dioxide, water and butane were detected at retention times of 1.52, 1.54, 2.41, 6.42 and 9.53 min [27]. The normalized total ion current (TIC) for  $\text{CO}$ ,  $\text{CO}_2$  and  $\text{H}_2\text{O}$  after time reaction 60 hours is presented in Table 2.

The typical corresponding experimental dependencies of butane, oxygen, carbon monoxide and carbon dioxide in time are plotted in Figure 8. The rate of degradation was estimated to obey pseudo-first-order kinetics, and hence the rate constant for degradation  $k$  was obtained from the first-order plot according to equation (3),

$$\ln(c/c_0) = kt \quad (3)$$

where  $c_0$  is the initial concentration,  $c$  is the concentration of butane after time ( $t$ ), and  $k$  is the first-order rate constant.

The photocatalytic degradation of butane was fitted by curves of the first-order kinetics; the corresponding rate constants are given in Table 2. Djeghri et al. [36] reported photoinduced oxidation of C2–C8 alkanes on  $\text{TiO}_2$  at ambient temperature. In general, they observed that alkanes ( $\text{C}_n\text{H}_{2n+2}$ ) formed ketones ( $\text{C}_n\text{H}_{2n}\text{O}$ ) and other aldehydes  $\text{C}_m\text{H}_{2m}\text{O}$  with  $2 < m < n$ . If the alkane was branched, the ketone was  $\text{C}_m\text{H}_{2m}\text{O}$  with  $3 < m < n$ . The reactivity of different types of carbon atoms followed the sequence:  $C_{\text{tertiary}} > C_{\text{quaternary}} > C_{\text{secondary}} > C_{\text{primary}}$ . Paper [8] shows, that in our case, the reactivity of butane is different and simpler – no intermediate

**Table 2** Rate constant  $k$  and TIC for  $\text{CO}$ ,  $\text{CO}_2$  and  $\text{H}_2\text{O}$  of  $\text{TiO}_2$ -graphene oxide

Sample	$k$ 365 nm [ $\text{h}^{-1}$ ]	$\text{CO}$ [TIC]	$\text{CO}_2$ [TIC]	$\text{H}_2\text{O}$ [TIC]	$k$ 400 nm [ $\text{h}^{-1}$ ]	$\text{CO}$ [TIC]	$\text{CO}_2$ [TIC]	$\text{H}_2\text{O}$ [TIC]
TiGO_000	0.02686	4.2	7.4	2.1	0.00959	7.2	8.1	2.3
TiGO_001	0.0158	3.7	9.1	0.8	0.00641	16.8	21.1	1.4
TiGO_005	0.01341	9.3	9.1	0.8	0.00451	9.5	12.8	0.8
TiGO_010	0.01356	10.5	11.4	0.7	0.00641	0.6	1.6	0.7
TiGO_050	0.02664	13.1	11.6	1.7	0.00774	1.7	4.7	0.2
TiGO_075	0.00911	8.9	10.6	2.1	0.00774	18.3	18.4	0.7
TiGO_100	0.03012	9.3	7.5	1.7	0.00739	12.4	15.4	0.7
TiGO_200	0.01663	6.7	13.2	1.1	0.00705	13.8	20.4	0.6
TiGO_300	0.00751	19.6	20.5	3.5	0.00517	14.7	19.5	0.8
TiGO_400	0.00683	9.1	9.6	1.9	0.00566	6.6	5.5	1.5
TiGO_500	0.00621	8.2	8.5	0.9	0.00512	6.1	4.9	0.9

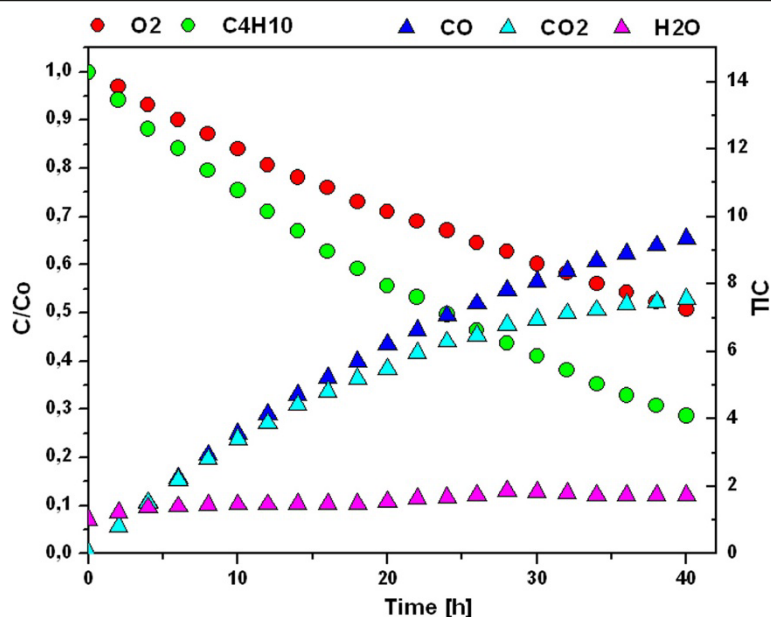


**Figure 8** Typical experimental dependencies of C<sub>4</sub>H<sub>10</sub>, O<sub>2</sub>, CO, CO<sub>2</sub> and H<sub>2</sub>O in time.

products such as lower alkane or ketones were detected in the gaseous phase. This means that photocatalytic oxidation proceeds not in the gaseous phase but only on the layer surface directly, causing formation of CO, CO<sub>2</sub> and H<sub>2</sub>O.

The results presented in Table 2 show, that the best photocatalytic activity under UV and visible light have samples denoted TiGO\_100 ( $k = 0.03012 \text{ h}^{-1}$ ) and TiGO\_075 ( $k = 0.00774 \text{ h}^{-1}$ ), respectively. As for the TiGO\_075 sample, there is also the largest increase in CO and CO<sub>2</sub> content. It is evident from Table 2 that for some samples, there is also an increase in CO and CO<sub>2</sub> at the expense of the primary decomposition of butane and the value for rate constant decreases. This suggests that in these samples a much deeper mineralization occurs, which leads to the preferential decomposition of intermediates to end products of photocatalytic decomposition, i.e. CO<sub>2</sub> and H<sub>2</sub>O. This increase in photoactivity for some samples is probably due to reduction of Ti<sup>4+</sup> to Ti<sup>3+</sup> and oxidation of free  $\pi$  - bonds during preparation. The interaction of CO<sub>2</sub> molecules with the excited states of Ti<sup>3+</sup>-O- leads to the formation of CO<sub>2</sub><sup>•-</sup> anion radicals [37]. The CO<sub>2</sub><sup>•-</sup> anion radicals readily react with poly(hydroxyethyl metacrylate), which leads to the formation of carbon monoxide due to its strong adsorption on Ti sites of the TiO<sub>2</sub> surface [8]. The functions of the graphene oxide sheets in the nanocomposite are as follows: i) graphene oxide sheets provide a very good support substrate for the deposition of TiO<sub>2</sub> nanoparticles, ii) graphene oxide sheets can enhance adsorption ability of the TiO<sub>2</sub> - graphene oxide nanocomposite, iii) Graphene oxide works as electron

acceptor and photosensitizer to efficiently enhance the butane photodecomposition.

## Conclusion

Using graphene oxide sheets as a substrate for TiO<sub>2</sub>, we developed a simple ("one-pot") method to prepare nanocomposite by depositing TiO<sub>2</sub> on the graphene oxide through liquid phase deposition.

The better photocatalytic properties on the TiO<sub>2</sub>-GO nanocomposite systems irrespective of light sources could be attributed to synergy effects including the increase in specific surface area with graphene oxide amount as well as to the formation of both  $\pi$ - $\pi$  conjugations between butane molecules and aromatic rings and the ionic interactions between butane and oxygen-containing functional groups at the edges or on the surfaces of carbon-based nanosheets. Graphene oxide works as the adsorbent, electron acceptor and photosensitizer and efficiently enhances the butane photodecomposition. The best photocatalytic activity under UV and visible light was observed for samples denoted TiGO\_100 ( $k = 0.03012 \text{ h}^{-1}$ ) and TiGO\_075 ( $k = 0.00774 \text{ h}^{-1}$ ), respectively. Both the used synthesis route and the GO modification are promising ways to cheap and efficient photocatalysts for the Vis light activation.

## Additional file

**Additional file 1: Figure S1.** The Raman spectrum of prepared graphene oxide. **Figure S2.** IR spectrum of the TiO<sub>2</sub>-GO nanocomposite.

**Figure S3.** UV-vis absorption spectra of the TiO<sub>2</sub>-GO. **Table S1.** C Composition of nanocomposite base on XPS.

#### Competing interests

The authors declare that they have no competing interests.

#### Authors' contributions

VŠ was the main author of the work, performed syntheses, and coordinated all characterization and catalytic studies. SB was responsible for electron microscopy, TMG for Raman spectroscopy, MK for XPS measurement, JB assisted with manuscript writing. All authors read and approved the final manuscript.

#### Acknowledgements

This work was supported by the RVO 61388980. The authors gratefully thank K. Šafářová (Regional Centre of Advanced Technologies and Materials, Faculty of Science, Palacký University in Olomouc) for AFM and TEM measurement.

#### Author details

<sup>1</sup>Department of Solid State Chemistry, Institute of Inorganic Chemistry AS CR v.v.i., Rež 250 68, Czech Republic. <sup>2</sup>Department of Physics, Faculty of Science, J.E.Purkyně University in Ústí nad Labem, Ústí n. L 400 96, Czech Republic.

Received: 10 December 2012 Accepted: 13 February 2013

Published: 27 February 2013

#### References

1. Krishnamoorthy K, Mohan R, Kim SJ: Graphene oxide as a photocatalytic material. *Appl Phys Lett* 2011, **98**(24).
2. Lambert TN, Chavez CA, Hernandez-Sanchez B, Lu P, Bell NS, Ambrosini A, Friedman T, Boyle TJ, Wheeler DR, Huber DL: Synthesis and characterization of titania-graphene nanocomposites. *J Phys Chem C* 2009, **113**(46):19812–19823.
3. Chen C, Cai W, Long M, Zhou B, Wu Y, Wu D, Feng Y: Synthesis of visible-light responsive graphene oxide/TiO<sub>2</sub> composites with p/n heterojunction. *ACS Nano* 2010, **4**(11):6425–6432.
4. Zhang Q, He Y, Chen X, Hu D, Li L, Yin T, Ji L: Structure and photocatalytic properties of TiO<sub>2</sub>-graphene oxide intercalated composite. *Chinese Sci Bull* 2011, **56**(3):331–339.
5. Min S, Lu G: Dye-sensitized reduced graphene oxide photocatalysts for highly efficient visible-light-driven water reduction. *J Phys Chem C* 2011, **115**(28):13938–13945.
6. Liang YT, Vijayan BK, Gray KA, Hersam MC: Minimizing graphene defects enhances titania nanocomposite-based photocatalytic reduction of CO<sub>2</sub> for improved solar fuel production. *Nano Lett* 2011, **11**(7):2865–2870.
7. Jiang G, Lin Z, Chen C, Zhu L, Chang Q, Wang N, Wei W, Tang H: TiO<sub>2</sub> nanoparticles assembled on graphene oxide nanosheets with high photocatalytic activity for removal of pollutants. *Carbon* 2011, **49**(8):2693–2701.
8. Stengl V, Popelkova D, Vlácil P: TiO<sub>2</sub>-graphene nanocomposite as high performance photocatalysts. *J Phys Chem C* 2011, **115**(51):25209–25218.
9. Stengl V: Preparation of graphene by using an intense cavitation field in a pressurized ultrasonic reactor. *Chem - Eur J* 2012. doi:10.1002/chem.201201411.
10. JCPDS: PDF 2 database, Release 50. Newtown Square: International Centre for Diffraction Data; 2000.
11. ICSD: ICSD Database. Germany: FIZ Karlsruhe; 2008.
12. Brunauer S, Emmett PH, Teller E: Adsorption of gases in multimolecular layers. *J Am Chem Soc* 1938, **60**:309–319.
13. Barrett EP, Joyner LG, Halenda PP: The determination of pore volume and area distributions in porous substances.1. Computations from nitrogen isotherms. *J Am Chem Soc* 1951, **73**(1):373–380.
14. Orel ZC, Gunde MK, Orel B: Application of the Kubelka-Munk theory for the determination of the optical properties of solar absorbing paints. *Prog Org Coat* 1997, **30**(1–2):59–66.
15. Stengl V, Houskova V, Bakardjieva S, Murafa N, Havlin V: Optically transparent titanium dioxide particles incorporated in poly(hydroxyethyl methacrylate) thin layers. *J Phys Chem C* 2008, **112**(50):19979–19985.
16. Stankovich S, Dikin DA, Piner RD, Kohlhaas KA, Kleinhammes A, Jia Y, Wu Y, Nguyen ST, Ruoff RS: Synthesis of graphene-based nanosheets via chemical reduction of exfoliated graphite oxide. *Carbon* 2007, **45**(7):1558–1565.
17. Wang GX, Yang J, Park J, Gou XL, Wang B, Liu H, Yao J: Facile synthesis and characterization of graphene nanosheets. *J Phys Chem C* 2008, **112**(22):8192–8195.
18. Jung HG, Myung ST, Yoon CS, Son SB, Oh KH, Amine K, Scrosati B, Sun YK: Microscale spherical carbon-coated Li<sub>4</sub>Ti<sub>5</sub>O<sub>12</sub> as ultra high power anode material for lithium batteries. *Energy Environ Sci* 2011, **4**(4):1345–1351.
19. Murafa N, Stengl V, Houskova V: Monodispersed spindle-like particles of titania. *Microsc Microanal* 2009, **15**:1036–1037.
20. Lowell S, Shields JE: *Powder Surface Area and Porosity*. 1998.
21. de Boer JA: *In Structure & Properties of Porous Materials*. 1958.
22. Ookubo A, Kanezaki E, Ooi K: ESR, XRD, and DRS studies of paramagnetic Ti<sup>3+</sup> ions in a colloidal solid of titanium-oxide prepared by the hydrolysis of TiCl<sub>3</sub>. *Langmuir* 1990, **6**(1):206–209.
23. Sereydych M, Bandosz TJ: Effects of surface features on adsorption of SO<sub>2</sub> on graphite oxide/Zr(OH)<sub>4</sub> composites. *J Phys Chem C* 2010, **114**(34):14552–14560.
24. Yang D, Velamakanni A, Bozoklu G, Park S, Stoller M, Piner RD, Stankovich S, Jung I, Field DA, Ventrice CA Jr, Ruoff RS: Chemical analysis of graphene oxide films after heat and chemical treatments by X-ray photoelectron and Micro-Raman spectroscopy. *Carbon* 2009, **47**(1):145–152.
25. Shao GS, Zhang XJ, Yuan ZY: Preparation and photocatalytic activity of hierarchically mesoporous-macroporous TiO<sub>2</sub>-xNx. *Appl Catal Environ* 2008, **82**(3–4):208–218.
26. Lam E, Chong JH, Majid E, Liu Y, Hrapovic S, Leung ACW, Luong JHT: Carbocatalytic dehydration of xylose to furfural in water. *Carbon* 2012, **50**(3):1033–1043.
27. Bentley FF, Smithson LD, Rozek AL: *Infrared Spektra and Characteristic Frequencies 700–300 cm<sup>-1</sup>*. New-York: Wiley-Interscience; 1968.
28. Zhang Y, Tang Z-R, Fu X, Xu Y-J: TiO<sub>2</sub>-graphene nanocomposites for gas-phase photocatalytic degradation of volatile aromatic pollutant: is TiO<sub>2</sub>-graphene truly different from other TiO<sub>2</sub>/Carbon composite materials? *ACS Nano* 2010, **4**(12):7303–7314.
29. Christy AA, Kvalheim OM, Velapoldi RA: Quantitative-analysis in diffuse-reflectance spectrometry - a modified Kubelka-Munk equation. *Vib Spectrosc* 1995, **9**(1):19–27.
30. Reddy KM, Manorama SV, Reddy AR: Bandgap studies on anatase titanium dioxide nanoparticles. *Mater Chem Phys* 2003, **78**(1):239–245.
31. Tauc J, Grigorov R, Vancu A: Optical properties and electronic structure of amorphous germanium. *Phys Status Solidi* 1966, **15**(2):627–637.
32. Serpone N, Lawless D, Khairutdinov R: Size effects on the photophysical properties of colloidal anatase TiO<sub>2</sub> particles - size quantization or direct transitions in this indirect semiconductor. *J Phys Chem* 1995, **99**(45):16646–16654.
33. Jeong HK, Jin MH, So KP, Lim SC, Lee YH: Tailoring the characteristics of graphite oxides by different oxidation times. *J Phys D: Appl Phys* 2009, **42**(6):Article number 065418.
34. Zhang Y, Pan C: TiO<sub>2</sub>/graphene composite from thermal reaction of graphene oxide and its photocatalytic activity in visible light. *J Mater Sci* 2011, **46**(8):2622–2626.
35. Lorences MJ, Patience GS, Diez FV, Coca J: Transient n-butane partial oxidation kinetics over VPO. *Appl Catal A-General* 2004, **263**(2):193–202.
36. Djeghri N, Formenti M, Juillet F, Teichner SJ: Photointeraction on surface of titanium-dioxide between oxygen and alkanes. *Faraday Discuss* 1974, **58**:185–193.
37. Sasirekha N, Basha SJS, Shanthy K: Photocatalytic performance of Ru doped anatase mounted on silica for reduction of carbon dioxide. *Appl Catal Environ* 2006, **62**(1–2):169–180.

doi:10.1186/1752-153X-7-41

Cite this article as: Štengl et al.: TiO<sub>2</sub>-graphene oxide nanocomposite as advanced photocatalytic materials. *Chemistry Central Journal* 2013 **7**:41.